

Inhibition of DNA replication initiation by silver nanoclusters

Yu Tao¹, Tomas Aparicio¹, Mingqiang Li², Kam W. Leong², Shan Zha^{1,3,4} and Jean Gautier^{1,4,5,*}

¹Institute for Cancer Genetics, Columbia University, New York, NY 10032, USA, ²Department of Biomedical Engineering, Columbia University, New York, NY 10027, USA, ³Departments of Pediatrics, Pathology and Cell Biology, Immunology and Microbiology, Columbia University, New York, NY 10032, USA, ⁴Herbert Irving Comprehensive Cancer Center, Columbia University, New York, NY 10032, USA and ⁵Department of Genetics and Development, Columbia University, New York, NY 10032, USA

Received September 27, 2020; Revised March 10, 2021; Editorial Decision March 31, 2021; Accepted April 07, 2021

ABSTRACT

Silver nanoclusters (AgNCs) have outstanding physicochemical characteristics, including the ability to interact with proteins and DNA. Given the growing number of diagnostic and therapeutic applications of AgNCs, we evaluated the impact of AgNCs on DNA replication and DNA damage response in cell-free extracts prepared from unfertilized *Xenopus laevis* eggs. We find that, among a number of silver nanomaterials, AgNCs uniquely inhibited genomic DNA replication and abrogated the DNA replication checkpoint in cell-free extracts. AgNCs did not affect nuclear membrane or nucleosome assembly. AgNCs-supplemented extracts showed a strong defect in the loading of the mini chromosome maintenance (MCM) protein complex, the helicase that unwinds DNA ahead of replication forks. FLAG-AgNCs immunoprecipitation and mass spectrometry analysis of AgNCs associated proteins demonstrated direct interaction between MCM and AgNCs. Our studies indicate that AgNCs directly prevent the loading of MCM, blocking pre-replication complex (pre-RC) assembly and subsequent DNA replication initiation. Collectively, our findings broaden the scope of silver nanomaterials experimental applications, establishing AgNCs as a novel tool to study chromosomal DNA replication.

INTRODUCTION

Silver nanomaterials are routinely incorporated into medical and consumer products due to their excellent antimicrobial capacities (1,2). Therefore, it is important to assess how they interact with macromolecules during biological processes such as DNA transactions to better understand their potential toxicity (3). The biological properties and potential toxic effects of silver nanomaterials are governed by multiple physicochemical factors including shape, size, dose and surface coating (4,5). Specifically, the impact of nanosilver is thought to be related to the release of silver ions, reactive oxygen production, and the direct interactions with biomacromolecules proteins and nucleic acid (6–10). Silver nanoclusters (AgNCs) have gained tremendous attention in recent years owing to the significant promises for fundamental research, as well as nanotechnology-based technological and biological applications (11,12). The outstanding physicochemical characteristics of AgNCs, including low cost, excellent dispersibility, easy preparation, facile functionalization, tunable emission wavelength, and high catalytic activity (13–16), have boosted their multidisciplinary applications in areas of catalysis (17,18), biosensing and disease diagnosis (19–21), biological imaging (22,23), biomedicine (24,25), antimicrobial agent (26), optoelectronics (27), and complex logic gates/logic device fabrications (13,28). The development of AgNCs-based applications also raises concerns regarding their potential toxicity.

AgNCs can be successfully synthesized by utilizing diverse templates, including DNA and proteins (29) since silver ions show high affinity to deoxyribonucleic acids, especially the cytosine base in DNA, as well as the Cys residues, N-terminal amine and metal-binding sites in proteins (30,31). In addition, ultrasmall AgNCs with extremely high surface-to-volume ratios are also expected to show significant interactions with proteins and DNA owing to their strong affinity to sulfur in proteins and heterocyclic bases of DNA, which may alter protein function, DNA conformation and potentially DNA transactions resulting in as-

*To whom correspondence should be addressed. Tel: +1 212 851 4564; Email: jg130@cumc.columbia.edu

Present addresses:

Yu Tao, Laboratory of Biomaterials and Translational Medicine, The Third Affiliated Hospital, Sun Yat-sen University, Guangzhou 510630, China.

Mingqiang Li, Laboratory of Biomaterials and Translational Medicine, The Third Affiliated Hospital, Sun Yat-sen University, Guangzhou 510630, China.

sociated genotoxicity (30,32). Although some toxicological studies on large-sized silver nanoparticles have been conducted (33–36), little is known about how AgNCs impact on complex biological reactions within cells. Moreover, the mechanisms by which AgNCs could impact DNA replication and DNA damage repair pathways are not known.

DNA replication is the essential process by which cells duplicate their genomes to ensure the maintenance of genetic information throughout cell divisions (37–40). Genome replication starts with the stepwise assembly of pre-replication complexes (pre-RCs) throughout the genome followed by the cell cycle dependent conversion and activation of a subset of pre-RCs into origins of replication (37–38,40). A key regulatory step to ensure that the genome is replicated only once per cell cycle is the loading and subsequent activation of the minichromosome maintenance (MCM) protein complex: these two processes are temporarily distinct (37,41–42). Activation of the MCM helicase requires the binding of CDC45 and the GINS protein complex, yielding a functional CMG DNA helicase complex (43–45). This activation step is the target of DNA damage checkpoints that prevent further firing in the presence of damaged templates or dysfunctional DNA polymerases. This DNA replication checkpoint is critical to maintain genomic integrity (39,46)

Here, we assessed the impact of silver nanoclusters (AgNCs) on essential DNA transactions to better understand how these nanoclusters might interfere with cell physiology. We elected to use cell-free extracts derived from *Xenopus laevis* eggs to monitor DNA replication and DNA replication checkpoint (47–50), processes that are highly conserved between *Xenopus laevis* and mammalian cells (49). We show that AgNCs, but not silver ions, silver nanoparticles (AgNPs) or silver nanoprisms (AgNPrs), inhibit DNA replication initiation by blocking MCM assembly, thus preventing the formation functional pre-RCs.

MATERIALS AND METHODS

Antibodies and chemicals

A commercial antibody was used to detect ORC1 in extracts: anti-ORC1 (clone TK1/2, cat.# sc-53391, Santa Cruz). Antibodies against ORC2, CDC6, MCM and RPA were generated against the corresponding polypeptides and previously described (51,52). Mouse anti-phospho-Histone H2AX (Ser139, JBW301 #05–636; Millipore), rabbit anti-histone H3 (#9715; Cell Signaling), rabbit anti-CHK1-pS345 (#2341; Cell Signaling) and mouse anti-phospho-ATM (Ser1981, #200-301-400 Rockland) were purchased from commercial sources.

Silver nitrate (AgNO₃, 99.9995%) and sodium borohydride (NaBH₄, 98%) were purchased from Alfa Aesar. Poly(acrylic acid) sodium salt 35 wt% (MW≈15 000) and 3-aminopropyltriethoxysilane (APTES) were obtained from Sigma-Aldrich. α-[³²P]dCTP was purchased from Amersham Biosciences. ANTI-FLAG[®] M2 Affinity Agarose Gel and aphidicolin were purchased from Sigma-Aldrich. SYBR-Gold was purchased from Molecular Probes. All reagents were of the analytical reagent grades and utilized as received. All samples were prepared using ultrapure water (18.2 MΩ; Millipore Co.).

Synthesis of poly(acrylic acid)-templated silver nanoclusters

AgNO₃ (4.9 mg) was mixed with the 3-aminopropyltriethoxysilane (APTES) solution in methanol (2 ml, 2%). The mixture was stirred in the dark at 25°C for 2 h. Then, the solution (41 μl) was added to PAA solution (MW ≈ 15 000, 40 ml, 0.12%) and reduced with NaBH₄. The solution was stirred in the dark at 25°C for 24 h.

Preparation of FLAG peptide-tagged silver nanoclusters

PAA-AgNCs (2 mM) were mixed dropwise with the FLAG peptide (5 mM, CGGMDYKDHDADYKDHDIDYKD DDDKSGSRRRRRRRRR). The mixture was continuously shaken at 4°C for 12 h to achieve complete absorption of the –SH group of the peptides to the surface of the silver nanoclusters. Peptide-tagged silver nanoclusters were washed three times with ultrapure water using centrifugation. Excess peptide was removed by centrifugating the solution through a 10 kDa membrane.

Synthesis of silver nanoparticles and silver nanoprisms: see Supplemental Methods.

Frog egg extract and demembrated sperm nuclei preparation

Xenopus frogs were handled in accordance with guidelines provided by the Institutional Animal Care and Use Committee at Columbia University. LSS, HSS and demembrated sperm nuclei (chromatin) were prepared as previously described (53). For LSS preparation, female *Xenopus* (Nasco) were injected subcutaneously with 50 U of pregnant mare serum gonadotropin (EMD Millipore) 3–7 days before extract preparation. Frogs were induced to lay eggs by subcutaneous injection of 800 U of human chorionic gonadotropin (Sigma-Aldrich). Good eggs were collected overnight and rinsed in 0.25× MMR (20 mM HEPES–KOH, pH 7.4, 400 mM NaCl, 1 mM MgSO₄, 2 mM CaCl₂ and 0.1 mM EDTA). The jelly coat was dissolved in 10 mM cysteine in 0.25× MMR, eggs were washed twice with 0.25× MMR, activated by addition of 1 μg/ml calcium ionophore A23187 (Sigma-Aldrich) for 5 min, and then washed twice with S buffer (50 mM HEPES–KOH, pH 7.5, 50 mM KCl, 2.5 mM MgCl₂, 250 mM sucrose and 2 mM β-mercaptoethanol). Eggs were crushed in polypropylene tubes at 10 000 rpm for 30 min at 4°C. The crude cytosol was collected with a syringe, supplemented with 20 μg/ml cytochalasin B (Sigma-Aldrich), and homogenized by rotation for 5 min at 4°C. The extract was then subjected to a high-speed spin in an ultracentrifuge (Optima X-100; Beckman-Coulter) in a swing-bucket rotor (TLS-55) for 30 min at 55 000 rpm at 4°C. The cytoplasmic layer and membrane layer fractions were collected and supplemented with 30 mM creatine phosphate, 150 μg/ml phosphocreatine kinase and 20 μg/ml cycloheximide. HSS extract was prepared by spinning the crude extract prepared as described at 55 000 rpm for 2.5 h. The clear, membrane-free HSS extract was recovered, carefully excluding the dense membrane layer below.

Demembrated sperm nuclei was prepared as described in (54). For nuclei isolation, 30 μl sperm-containing aliquots were diluted in 800 μl ice-cold chromatin isolation

buffer (50 mM HEPES–KOH, pH 7.8, 100 mM KCl and 2.5 mM MgCl₂) supplemented with 0.125% Triton X-100 and overlaid onto 30% sucrose (wt/vol) chromatin isolation buffer. Samples were spun at 10 000 rpm for 30 min at 4°C in a swing-bucket rotor (HB-6; Sorval). The final pellet was re-suspended in SDS-PAGE loading buffer, resolved on a 10% SDS-PAGE gel and analyzed by immunoblotting.

DNA replication assay

DNA replication reactions contain 10 µl LSS extracts and demembrated sperm nuclei (2000 nuclei/µl) were supplemented with α-[³²P]dCTP and different Ag nanomaterials (AgNCs, Ag⁺, AgNPs, AgNPrs) with the same equivalent Ag concentration (20 µg ml⁻¹). The reactions were incubated at 21°C for 90 min. For DNA replication time-courses, AgNCs were added at the indicated timepoints. The reaction was then stopped by addition of stop buffer (50 mM Tris pH 8.0, 5 mM EDTA and 0.1% SDS). Genomic DNA was isolated by proteinase K digestion at 37°C for 2 h followed by phenol/chloroform extraction and ethanol precipitation. DNA pellets were resuspended in 20 µl TE buffer and ran on a 0.8% TBE–agarose gel, fixed in 30% trichloroacetic acid, dried by pressing between Whatman 3MM Chromatography Paper and paper towels overnight, and exposed for autoradiography. Signal quantification was performed using the ‘Analyze Gel’ tool in ImageJ (<http://rsb.info.nih.gov/ij/index.html>).

DNA damage repair assay

10 µl LSS extracts were mixed with demembrated sperm nuclei (2000 nuclei/µl) at 21°C for 15 min. Aphidicolin with different Ag nanomaterials (AgNCs, Ag⁺, AgNPs, AgNPrs) with the same equivalent Ag concentration (20 µg ml⁻¹) or PAA (960 µg ml⁻¹) were added to the mixture for additional 30 min incubation. Activation of DNA damage repair was monitored by Chk1 phosphorylation. Phosphorylated Chk1 protein was resolved on a 3–8% Tris-acetate NuPAGE gel according to the manufacturer’s instructions (Invitrogen, Carlsbad, CA, USA).

Nuclear assembly

Sperm nuclei were incubated in *Xenopus* egg extracts (2000/µl) for 15 min before AgNCs were added into the reactions for another 30 min at 21°C. The extent of nuclear assembly was monitored by mixing 1 µl extract sample with 1 µl Hoechst 33258 (20 µg/ml) and immediate observation under fluorescence microscope using a UV filter.

Micrococcal nuclease digestion assay

Reactions were performed in HSS extracts (10 µl) containing 3000 sperm nuclei/µl. The mixtures were incubated at 21°C for 20 min to allow chromatin assembly. 5 mM CaCl₂ and 100 units of Micrococcal nuclease were then added to each sample. Extract were incubated at 21°C and aliquots were sampled at 2, 4, 8, 10 min and diluted with 200 µl Stop Buffer (20 Mm Tris, pH 7.5, 30 mM EDTA, 0.5% SDS). Proteinase K (500 µg/ml) was then added to each sample and incubated at 37°C for 2 h. After that, 1 Volume of

phenol–chloroform saturated with TE was added to each sample, and centrifuged at 15 000 rpm for 4 min. The aqueous phase was then transferred to a new tube. DNA was precipitated by addition of 20 µl sodium acetate (3 M, pH 5.5) and 5 volumes cold ethanol, and pelleted centrifugation for 10 min. The DNA pellet was resuspended in 15 µl TE buffer run on a 1.5% TBE–agarose gel and stained using SYBR gold following manufacturer instructions.

Chromatin binding assays

For chromatin binding experiments, 15 µl LSS extract was supplemented with demembrated sperm nuclei (2500 sperm/µl) and incubated for 10 min at 21°C to allow chromatin assembly. For the time-course chromatin binding assays, AgNCs were added at the indicated timepoints. The reaction was then stopped at different times by diluting with the chromatin isolation buffer (50 mM HEPES–KOH, pH 7.8, 100 mM KCl, 2.5 mM MgCl₂, 0.125% Triton-X100). The extracts were overlaid on top of 30% sucrose cushions in 1.5 ml protein low-retention tubes (Thermo Fisher Scientific). Samples were spun at 7800 rpm in HB-6 rotor for 30 min at 4°C. Chromatin pellets were resuspended in 10 µl Laemmli buffer, boiled at 90°C for 60 s and fractionated on a 3–8% gradient Tris–acetate gels (Invitrogen) according to standard procedures, followed by transfer of resolved proteins onto PVDF membranes (EMD Millipore). Following a 1 h block with 5% non-fat dried milk in PBS, membranes were incubated overnight at 4°C with one of the following primary antibodies: ORC1, ORC2, CDC6, MCM3 (52), CDC6, RPA32 and histone H3. HRP-conjugated secondary antibodies (anti-rabbit IgG HRP, anti-mouse IgG HRP, Fisher Scientific) and chemiluminescence (SuperSignal West Pico Chemiluminescent Substrate, 34077) were used.

Immunoprecipitation assay

For immunoprecipitations, FLAG-tagged AgNCs were incubated in 50 µl of LSS extract at 21°C. Extracts were diluted in 50 µl IP buffer (1 × ELB salts, 0.25 M sucrose, 75 mM NaCl, 2 mM EDTA, 10 µg/ml aprotinin/leupeptin, 0.1% NP-40) and supplemented with 10 µl pre-washed FLAG M2 agarose beads (Sigma-Aldrich). Beads were incubated in *Xenopus* extract for 2 h at 4°C and subsequently washed using 2.5 ml IP buffer. Beads were taken up in 15 µl of 2× SDS sample buffer and incubated for 5 min at 95°C. Proteins were loaded on SDS–PAGE and visualized by western blot with the indicated antibodies.

Mass spectrometry

FLAG-tagged AgNCs were incubated in *Xenopus* egg extracts, then affinity-purified and subsequently subjected to mass spectrometric analysis of AgNCs associated proteins applying quantitative mass spectrometry (see Supporting Information).

RESULTS AND DISCUSSION

Poly(acrylic acid) (PAA)-templated AgNCs (Figure 1A) were synthesized according to a modified protocol previ-

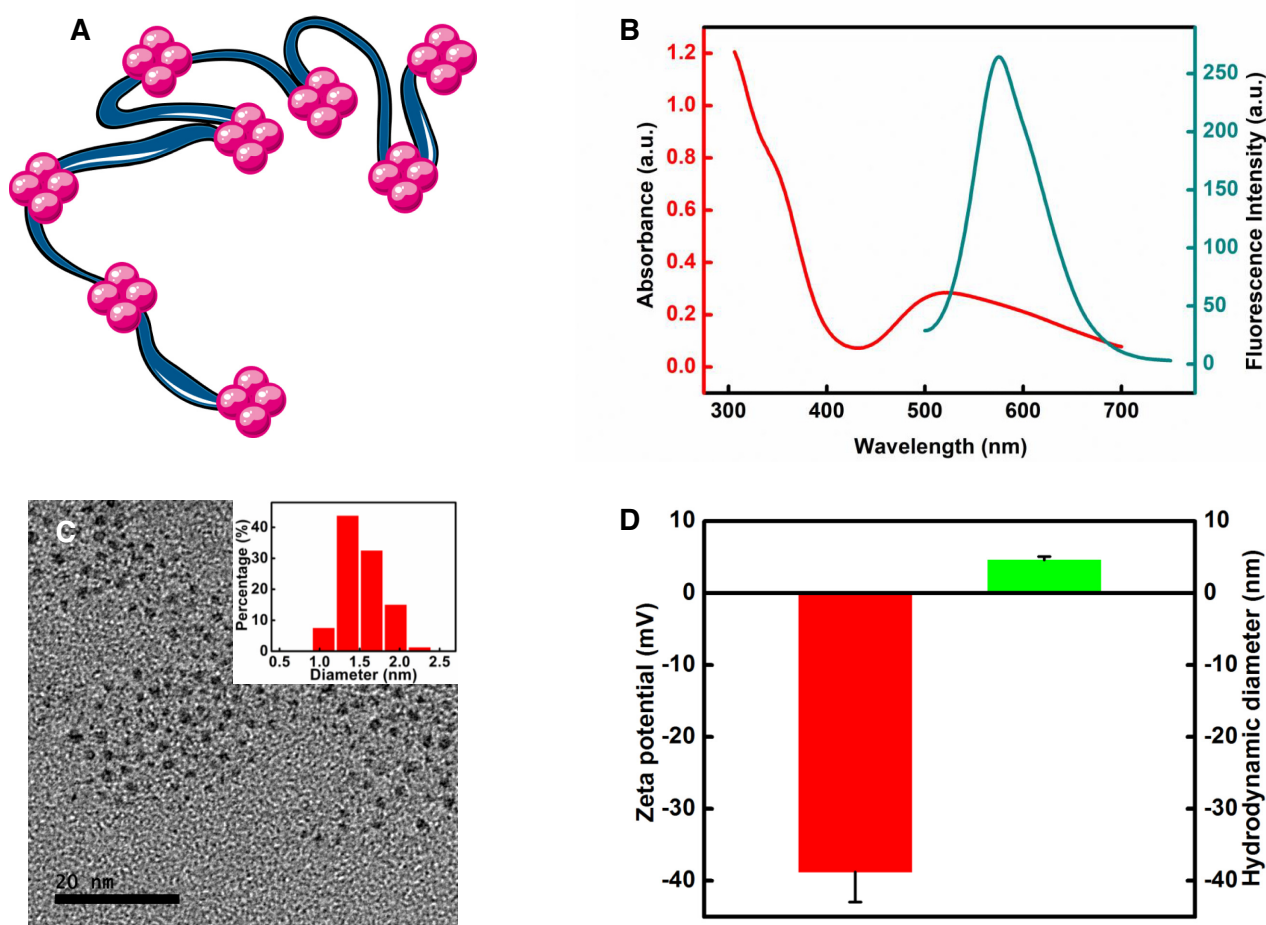


Figure 1. Synthesis and characterization of silver nanoclusters (AgNCs). (A) Schematic diagram of AgNCs. (B) Absorbance and fluorescence spectra of AgNCs. (C) Transmission electron microscopy (TEM) image and corresponding size distribution histogram of AgNCs. Scale bars, 20 nm. (D) Zeta potential and hydrodynamic diameter of AgNCs.

ously described (55). Successful generation of AgNCs was confirmed by: (i) optical absorption; (ii) fluorescence characteristic and (iii) transmission electron microscopy (TEM). As shown in Figure 1B, AgNCs exhibit characteristic absorption peaks at 350 and 515 nm (56). The fluorescent spectrum reveals that AgNCs displayed a strong emission peak at 575 nm and were stable for several months (data not shown). Figure 1C shows a typical TEM image of the AgNCs prepared as described, in which AgNCs were monodispersed and uniform with an average size of about 1.54 nm (57,58). Dynamic light scattering (DLS) characterization indicates that zeta potential and hydrodynamic diameter of AgNCs were -38.8 ± 4.2 mV and 4.6 ± 0.5 nm, respectively (Figures 1D). DLS measurements of AgNCs showed a slightly increased diameter as compared to TEM imaging, which could result from dehydration of AgNCs in sample preparation for TEM observations (59,60). Similarly, silver nanoparticles (AgNPs) and silver nanoprisms (AgNPrs) were characterized by optical absorption, fluorescence and TEM (Supplementary Figure S1).

First, we sought to investigate the impact of AgNCs, Ag^+ , AgNPs and AgNPrs on DNA transactions, given their properties to interact with DNA and proteins. Cell-free extracts prepared from unfertilized *Xenopus laevis* eggs faithfully recapitulate, cell cycle-regulated, genomic DNA replication (47–50). Specifically, we and others have studied the stepwise assembly and activation of the pre-RC in these extracts (51–52,61–63). Thus, we investigated first the effects of AgNCs on DNA replication and DNA replication checkpoint, a physiological consequence of stalling DNA replication forks. We used low-speed supernatant (LSS) extracts from *Xenopus laevis* eggs to monitor genomic DNA replication (Figure 2A, control). The addition of increasing concentrations of AgNCs to extracts concomitant with the addition of demembrated sperm nuclei abrogated DNA replication as seen by the inhibition of α - ^{32}P dCTP incorporation into chromosomal DNA (Figure 2a and b). We then tested whether AgNCs could also inhibit the DNA replication checkpoint. AgNCs showed good stability in replication assay buffer (Supplementary Figure S2). Upon

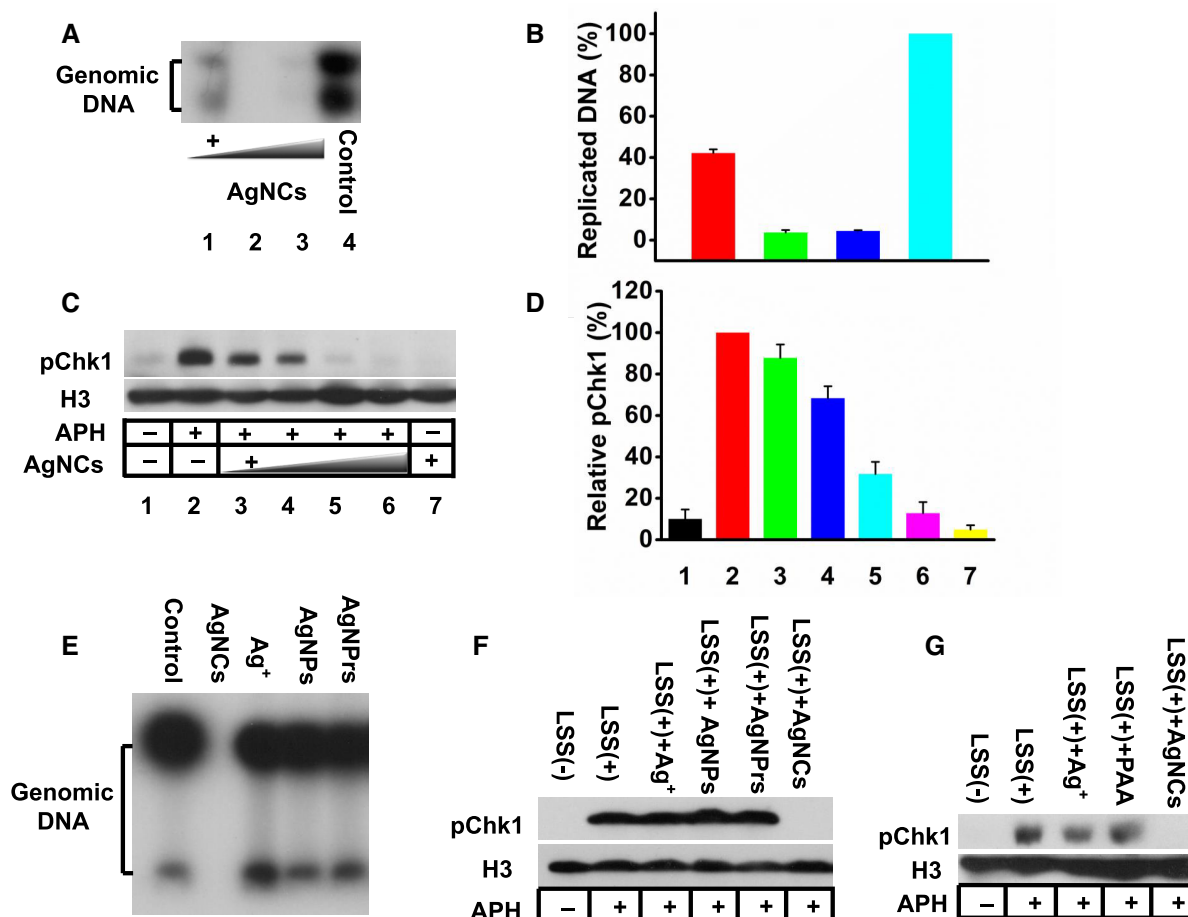


Figure 2. AgNCs uniquely inhibit DNA replication and replication checkpoint. (A, B) DNA replication in extracts is sensitive to AgNCs. (A) *Xenopus* egg extracts were incubated with sperm nuclei in the presence of increasing concentrations of AgNCs. DNA replication was monitored by agarose gel electrophoresis after incorporation of α - 32 P]dCTP into genomic DNA. (B) Quantification of three independent experiments normalized to untreated controls. (C, D) AgNCs inhibit the DNA replication checkpoint. (C) *Xenopus* egg extracts were treated with aphidicolin with or without AgNCs at different concentrations and incubated with sperm nuclei. ATR activation was monitored by pChk1 western blotting. (D) Quantification of three independent experiments normalized to aphidicolin alone control. Impact of different silver nanomaterials on DNA replication and replication checkpoint. (E) Replicating extracts were incubated with silver ions (Ag^+), silver nanoparticles (AgNPs), silver nanoprisms (AgNPrs) and silver nanoclusters (AgNCs) and DNA replication was assessed by incorporation of α - 32 P]dCTP into genomic DNA. (F, G) The impact of Ag^+ , AgNPs, AgNPrs AgNCs and PAA on DNA replication checkpoint was monitored by pChk1 Western blotting.

inhibition of DNA replication fork progression, single-stranded DNA is generated as a result of DNA helicase uncoupling and the ATR-Chk1 signaling pathway, a key effector of DNA replication checkpoints is activated (64). A critical substrate of ATR is the protein serine-threonine checkpoint kinases Chk1, which triggers a broad range of downstream responses (65). To confirm DNA replication inhibition, we monitored Chk1 phosphorylation (pChk1) at serine 343 (S345 in human) as a readout for activation of the replication checkpoint by ATR. In this experimental setup, the replication checkpoint is triggered by addition of aphidicolin, an inhibitor of DNA polymerases (66). Consistent with DNA replication blockade (Figure 2A) pChk1 signal progressively decreased with increasing concentrations of AgNCs (Figure 2C and D), strengthening the idea that AgNCs inhibit DNA replication and subsequent checkpoint signaling.

Silver ions and several silver-based nanomaterials display toxicity (3,6,8). Therefore, we sought to determine whether

other silver materials could inhibit DNA replication in cell-free extracts. We employed four different types of silver materials, including silver ions, silver nanoparticles (Supplementary Figure S1a-c), silver nanoprisms (Supplementary Figure S1d-f) and silver nanoclusters. We reasoned that in addition to providing information on the role of silver ions, we could obtain insights on the mechanisms of DNA replication inhibition by AgNCs related to the geometry of the silver nanomaterials. Notably, we find that only silver nanoclusters efficiently inhibited DNA replication and checkpoint signaling (Figures 2E, second lane and Figure 2F, last lane, Supplementary Figure S3), which strongly argued against the possibility that inhibition of DNA replication was due to silver ions toxicity. These data also indicate that the morphology of AgNCs is critical for their impact on DNA replication and signaling. We also tested whether distinct nanomaterials with comparable size of AgNCs could inhibit DNA replication in cell-free extracts. We compared four different types of nanomaterials: gold

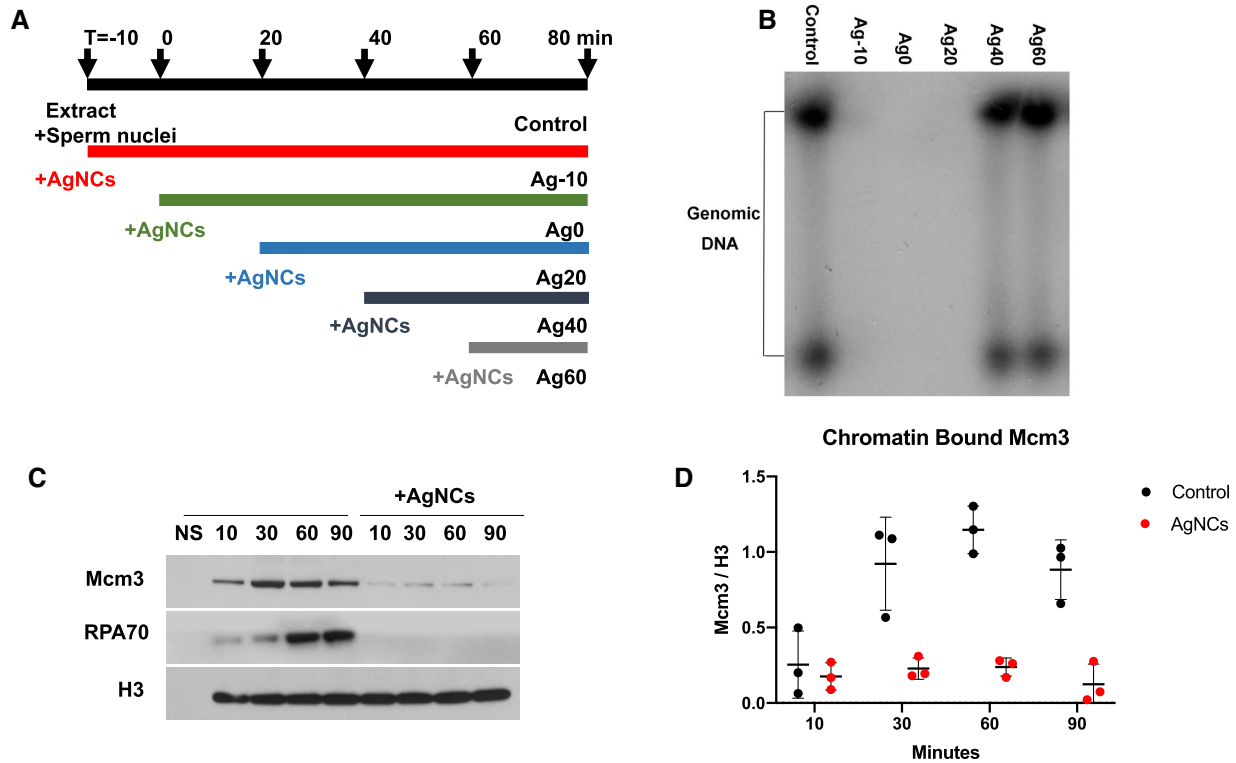


Figure 3. AgNCs affect DNA replication initiation. (A, B) Time-course of DNA replication assay. (A) Experiment time-course showing the time of AgNCs addition to DNA replication assay. (B) AgNCs were added to extracts at different time points during DNA replication ($T = -10, 0, 20, 40, 60$ min) and DNA replication products were monitored by agarose gel electrophoresis at 80 min after addition of AgNCs. For the first lane (control), no AgNCs were added and replication was monitored at 80 min. (C, D) AgNCs block pre-RC assembly. (C) Chromatin binding assays were performed in *Xenopus* egg extracts supplemented with demembranated sperm nuclei (2500 sperm/ μ l) and incubated for 10 min at 21°C for chromatin assembly following addition of AgNCs at indicated timepoints (10, 30, 60 and 90 min). Chromatin was isolated through 30% sucrose cushions and bound proteins were resolved by SDS-PAGE on 10% Bis-Tris gels and probed with specific antibodies against MCM3, RPA and histone H3. (D) The mean and standard deviation is shown for three independent biological replicates.

nanoclusters, copper nanoclusters, carbon dots and AgNCs. Notably, we found that only AgNCs efficiently inhibited DNA replication (Supplementary Figures S4a) and downstream signaling (Supplementary Figures S4b). This strongly suggests a AgNCs-specific effect on DNA replication. To further establish that the geometry of AgNCs was critical, we also tested the impact of the PAA synthesis template on checkpoint signaling (Figure 2G), showing no influence on pChk1 signals. In summary, the data suggest that inhibition of DNA replication is due to the inherent geometry and characteristics of AgNCs.

Nuclear assembly is a prerequisite for efficient DNA replication in cell-free extracts (50,67). Microscopic observation of nuclear assembly indicated that nuclei formation, i.e. the transition from compact ‘worm-like’ demembranated sperm nuclei into near spherical nuclei harboring a nuclear membrane, was not affected by AgNCs (Supplementary Figure S5). We also digested chromatin prepared from control and AgNCs-treated extracts with micrococcal nuclease to analyze the impact of AgNCs on nucleosome assembly (Supplementary Figure S6) (68). We observed a similar nucleosome ‘ladder’ pattern in control and AgNCs-supplemented extracts, indicating that AgNCs did not impair nucleosome assembly (69).

DNA replication initiation and elongation proceed synchronously in cell-free extracts. Thus, in an attempt to distinguish whether AgNCs inhibited an early vs. late replication step, we added AgNCs at various times during the process (Figure 3A). When added at the time of nuclei addition (–10) or at 0 or 20 min, AgNCs completely inhibited genomic DNA replication. In contrast, the addition of AgNCs at 40 or 60 min had no impact on genomic DNA replication as seen by the incorporation of α -[32 P]dCTP (Figure 3B). This suggests that AgNCs block an early step, such as DNA replication initiation but do not affect DNA replication elongation.

Next, to gain further mechanistic insights into the mechanism of replication inhibition, we tested whether AgNCs impaired the assembly of the pre-replication complex (pre-RC). The synchronous nature of pre-RC assembly and activation in extracts facilitates the biochemical study of these processes by monitoring chromatin-bound replication factors (50). Origin assembly starts with the loading of the origin recognition complex (ORC) in G1 followed by the sequential loading of cell division cycle 6 (Cdc6) which, together with chromatin licensing and DNA replication factor 1 (Cdt1), allow the assembly of minichromosome maintenance complex proteins 2–7 (MCM2–7) (70), thus com-

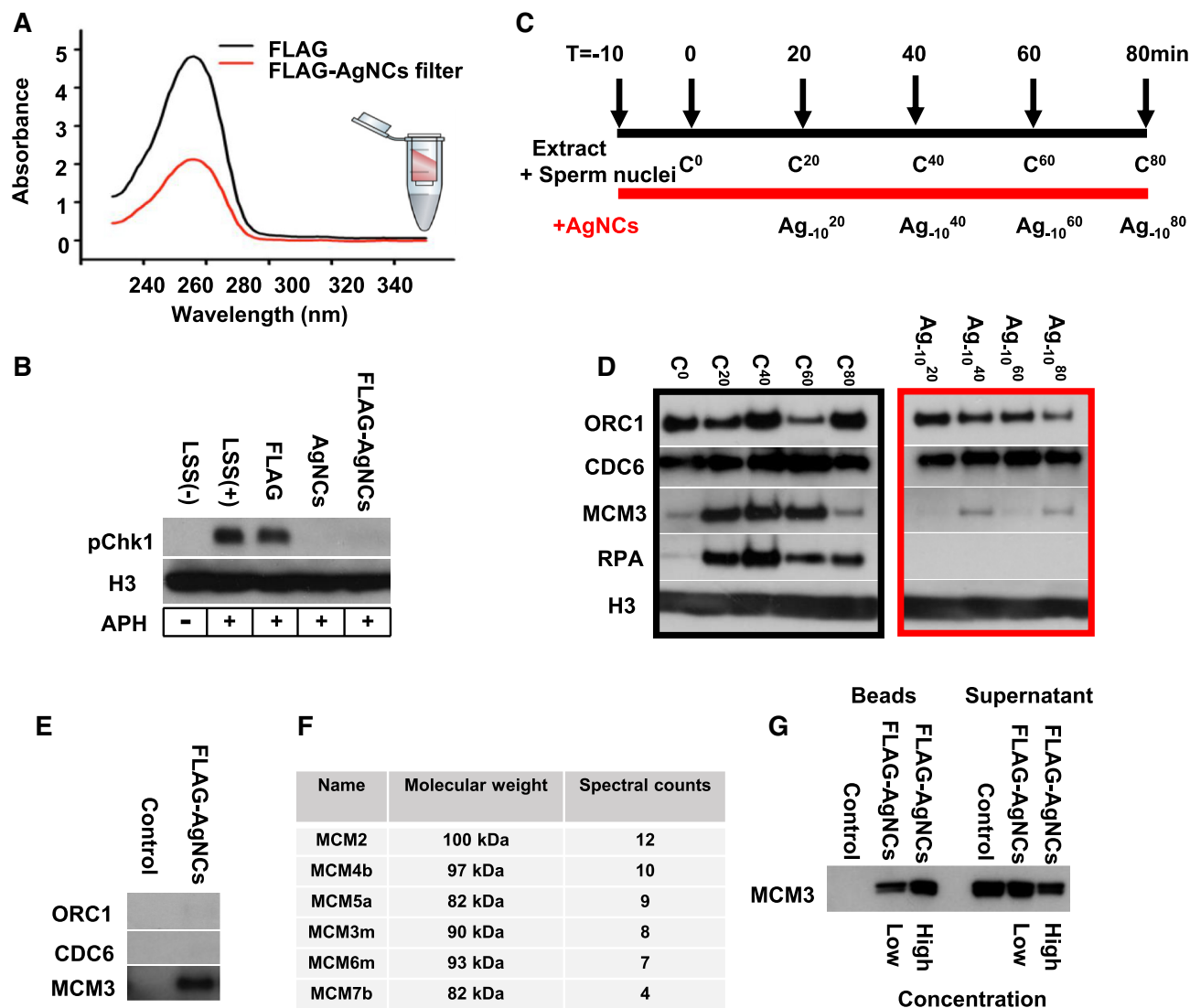


Figure 4. AgNCs interact with MCM protein complex. (A) Synthesis of FLAG-AgNCs (FLAG peptide: CGGMDYKDHDADYKDHDIDYKDDDDK). The decrease of FLAG peptide absorbance in the filter indicated the successful linkage of FLAG peptide on AgNCs. (B) FLAG-tagged AgNCs inhibits the DNA replication checkpoint. *Xenopus* egg extracts were treated with aphidicolin with or without AgNCs or FLAG-AgNCs and incubated with sperm nuclei. ATR activation was monitored by pChk1 western blotting. (C, D) Chromatin binding assay in the presence of FLAG-AgNCs. (C) Schematic representation of the experiments. (D) Chromatin was isolated through 30% sucrose cushion and bound proteins (ORC1, CDC6, MCM3, RPA and histone H3) resolved by 3%-8% gradient Tris-Acetate gels followed by western blot. Left: control, untreated extracts. Right: extracts incubated with FLAG-tagged AgNCs. (E) *Xenopus* egg extracts were incubated with FLAG peptide (control) or FLAG-AgNCs, immunoprecipitated with anti-FLAG antibodies, washed and processed for western blot with ORC1, CDC6 and MCM3 antibodies. (F) *Xenopus* egg extracts were incubated for 1 h with FLAG-AgNCs. Following FLAG immunoprecipitation, AgNCs-bound proteins were identified by mass spectrometry. MCM polypeptides recovered are indicated. (G) Purified hexameric MCM complex expressed in baculovirus-infected cells was incubated with FLAG-AgNCs *in vitro*. Bound and soluble fractions were processed for Western blotting with MCM3 antibodies.

pleting pre-RC assembly. At the onset of DNA replication, conversion of the pre-RC into an initiation complex, Cdc45 and the GINS complex bind to the hexameric MCM complex, yielding an active CMG helicase (41,43,71). Following DNA unwinding, the heterotrimeric protein complex replication protein A (RPA) binds single-strand DNA with high affinity (72). Using specific antibodies previously described (51,52), we first monitored chromatin binding of MCM (MCM3), a key pre-RC component, and RPA, a readout of the activation of the replicative helicase (Figure 3C, D and Supplementary Figure S7). We used histone H3

as a chromatin loading control. Nuclei were allowed to assemble for 10 min in extracts, then chromatin was isolated and processed for western blotting at 10, 30, 60 and 90 min. As previously reported, we observed time-dependent loading of MCM followed by the subsequent assembly of RPA on ssDNA (Figure 3C). In presence of AgNCs, MCM and RPA loading were strongly inhibited. A representative western blot is shown in Figure 3C and the normalized MCM values (to histone H3 loading controls) from three independent biological replicates are graphed (Figure 3D). AgNCs significantly inhibited MCM loading at 30, 60 and 90 min (*P*

< 0.001 at 60 min). In contrast the loading of ORC 1, 2 and CDC6 which takes place prior to MCM loading was unaffected by AgNCs (Supplementary Figure S7). When AgNCs was added at the beginning of the experiment (Ag₀), chromatin-bound ORC1, ORC2 and CDC6 were present at similar levels as in controls (no AgNCs). In contrast, MCM3 and RPA loading was inhibited. When AgNCs were added at later timepoints, MCM3 and RPA chromatin loading were gradually restored (Ag₂₀, Ag₄₀) (Supplementary Figure S7). Altogether, these data strongly suggest that AgNCs specifically prevent MCM loading.

Next, we wanted to assess whether AgNCs interact with MCM proteins, which could provide a mechanism for the inhibition of MCM chromatin loading. To this aim, we generated a tagged version of AgNCs. We synthesized a FLAG peptide-tagged AgNCs (FLAG-AgNCs, Figure 4A, Supplementary Figure S8). As seen in Figure 4B, FLAG-AgNCs was equally effective at inhibiting the DNA replication checkpoint elicited by aphidicolin as AgNCs. In addition, FLAG-AgNCs-treated extracts failed to properly assemble MCM and subsequently load RPA onto chromatin (Figure 4C, D). These results indicated that the FLAG addition did not alter the properties of AgNCs with regards to DNA replication and checkpoint inhibition.

Next, we performed pull-down assays to determine whether MCM proteins interact with AgNCs. Immunoprecipitation of FLAG-AgNCs following incubation in *Xenopus* cell-free extracts were performed followed by western blotting with MCM3 antibodies (Figure 4E). MCM3 was readily detected on beads bound to FLAG-AgNCs but not in control (FLAG only) beads. In contrast, we could not detect ORC or CDC6 in these pull-downs. Next, to independently confirm these observations, we performed immunoprecipitation of FLAG-AgNCs followed by mass spectrometry. FLAG-tagged AgNCs were incubated in cell-free extracts, affinity-purified and subsequently subjected to mass spectrometric analysis (see Materials and Methods). As shown in Figure 4F, all six subunits of the MCM complex proteins were identified in the AgNCs immunoprecipitates, confirming the affinity of AgNCs to MCM proteins by an unbiased approach.

Finally, we wanted to test whether AgNCs interacted directly with the hetero-hexameric MCM complex. Recombinant MCM protein complex purified from baculovirus infected cells (51) was incubated with AgNCs beads or control beads followed by western blot with MCM3 antibodies (Figure 4G). We could observe direct interaction of AgNCs with the MCM complex. Furthermore, incubation with higher concentrations of FLAG-AgNCs yielded a stronger MCM signal in the bound fraction together with a decreased MCM signal in the soluble, unbound fraction.

The hexameric MCM2–7 complex has a molecular mass of about ~560 kDa and a globular shape (13 × 19 nm), which contains a central channel with a diameter of 3–4 nm and a smaller side channel (73). Soluble MCM2–7 hexamer forms a flexible open-ringed structure bound to CDT1. This complex strongly interacts with ORC-CDC6 bound to DNA via the C-terminal extensions of MCM polypeptides. Subsequently, two MCM rings interacts on DNA in a head-to-head configuration via the N-terminal domains of MCM proteins, a process facilitated by CDT1 removal

(42,74). AgNCs could interact with the internal cavity of MCM open-ringed structure and prevent interaction with ORC-CDC6 at DNA-bound origins. Alternatively, AgNCs could interfere with the interface between MCM ring, thus destabilizing the dimers and preventing the assembly of a functional helicase. Our laboratory has previously demonstrated that the MCM complex's intrinsic DNA helicase activity is dispensable for its loading as hexameric complex on DNA (51). Therefore, we favor the idea that AgNCs alter MCM-DNA interactions rather than DNA unwinding itself. Further structural studies of the AgNCs–hexameric MCM complex are warranted to establish the exact mechanism of inhibition by AgNCs.

In summary, this study provides an example of specific interaction between one type of silver nanomaterial and an essential nuclear protein complex. This in turn, sheds light on a possible mechanism for AgNCs toxicity. Notably, this study could serve as a starting point to develop inhibitors of the MCM protein complex for both experimental and therapeutic applications (75).

DATA AVAILABILITY

Proteomics dataset are available at: <https://massive.ucsd.edu/ProteoSAFe/dataset.jsp?accession=MSV000086216>.

SUPPLEMENTARY DATA

Supplementary Data are available at NAR Online.

ACKNOWLEDGEMENTS

Mass Spectrometry analysis was performed at the Herbert Irving Comprehensive Cancer Center Proteomics and Macromolecular Crystallography Shared Resources at Columbia University Irving Medical Center.

FUNDING

NIH [R50 CA233182 to TA]; NIH [P01-CA174653 to J.G. and S.Z. and R35-CA197606 to J.G.]; National Natural Science Foundation of China [21907113, 51903256]; Guangdong Provincial Pearl River Talents Program [2019QN01Y131 to Y.T.]. Funding for open access charge: NCI Grant [R35CA197606].

Conflict of interest statement. None declared.

REFERENCES

- Eckhardt,S., Brunetto,P.S., Gagnon,J., Priebe,M., Giese,B. and Fromm,K.M. (2013) Nanobio silver: its interactions with peptides and bacteria, and its uses in medicine. *Chem. Rev.*, **113**, 4708–4754.
- Schnaider,L., Toprakcioglu,Z., Ezra,A., Liu,X.Z., Bychenko,D., Levin,A., Gazit,E. and Knowles,T.P.J. (2020) Biocompatible hybrid organic/inorganic microhydrogels promote bacterial adherence and eradication in vitro and in vivo. *Nano Lett.*, **20**, 1590–1597.
- House,J.S., Bouzouk,E., Fahy,K.M., Francisco,V.M., Lloyd,D.T., Wright,F.A., Motsinger-Reif,A.A., Asuri,P. and Wheeler,K.E. (2020) Low-dose silver nanoparticle surface chemistry and temporal effects on gene expression in human liver cells. *Small*, **16**, e2000299.
- AshaRani,P.V., Low Kah Mun,G., Hande,M.P. and Valiyaveetil,S. (2009) Cytotoxicity and genotoxicity of silver nanoparticles in human cells. *ACS Nano*, **3**, 279–290.

5. Ferdous, Z. and Nemmar, A. (2020) Health impact of silver nanoparticles: a review of the biodistribution and toxicity following various routes of exposure. *Int. J. Mol. Sci.*, **21**, 2375.
6. Ivask, A., ElBadawy, A., Kaweeteerawat, C., Boren, D., Fischer, H., Ji, Z.X., Chang, C.H., Liu, R., Tolaymat, T., Telesca, D. et al. (2014) Toxicity mechanisms in *Escherichia coli* vary for silver nanoparticles and differ from ionic silver. *ACS Nano*, **8**, 374–386.
7. Xiu, Z.-m., Zhang, Q.-b., Puppala, H.L., Colvin, V.L. and Alvarez, P.J.J. (2012) Negligible Particle-Specific antibacterial activity of silver nanoparticles. *Nano Lett.*, **12**, 4271–4275.
8. Park, M.V.D.Z., Neigh, A.M., Vermeulen, J.P., de la Fonteyne, L.J.J., Verharen, H.W., Briedé, J.J., van Loveren, H. and de Jong, W.H. (2011) The effect of particle size on the cytotoxicity, inflammation, developmental toxicity and genotoxicity of silver nanoparticles. *Biomaterials*, **32**, 9810–9807.
9. Nam, S.-H. and An, Y.-J. (2019) Size- and shape-dependent toxicity of silver nanomaterials in green alga *Chlorococcum infusionum*. *Ecotoxicol. Environ. Saf.*, **168**, 388–393.
10. Akter, M., Sikder, M.T., Rahman, M.M., Ullah, A., Hossain, K.F.B., Banik, S., Hosokawa, T., Saito, T. and Kurasaki, M. (2018) A systematic review on silver nanoparticles-induced cytotoxicity: physicochemical properties and perspectives. *J. Adv. Res.*, **9**, 1–16.
11. Shamsipur, M., Molaie, K., Molaabasi, F., Hosseinkhani, S., Taherpour, A., Sarparast, M., Moosavifard, S.E. and Barati, A. (2019) Aptamer-based fluorescent biosensing of adenosine triphosphate and cytochrome c via aggregation-induced emission enhancement on novel label-free DNA-capped silver nanoclusters/graphene oxide nanohybrids. *ACS Appl. Mater. Interfaces*, **11**, 46077–46089.
12. Shen, J., Wang, Z., Sun, D., Xia, C., Yuan, S., Sun, P. and Xin, X. (2018) pH-responsive nanovesicles with enhanced emission co-assembled by Ag(I) nanoclusters and polyethyleneimine as a superior sensor for Al(3). *ACS Appl. Mater. Interfaces*, **10**, 3955–3963.
13. Lv, M., Zhou, W., Fan, D., Guo, Y., Zhu, X., Ren, J. and Wang, E. (2020) Illuminating diverse concomitant DNA logic gates and concatenated circuits with hairpin DNA-templated silver nanoclusters as universal dual-output generators. *Adv. Mater.*, **32**, e1908480.
14. Xie, Z., Sun, P., Wang, Z., Li, H., Yu, L., Sun, D., Chen, M., Bi, Y., Xin, X. and Hao, J. (2020) Metal-organic gels from silver nanoclusters with aggregation-induced emission and fluorescence-to-phosphorescence switching. *Angew. Chem. Int. Ed. Engl.*, **59**, 9922–9927.
15. Guo, Y., Pan, X., Zhang, W., Hu, Z., Wong, K.W., He, Z. and Li, H.W. (2020) Label-free probes using DNA-templated silver nanoclusters as versatile reporters. *Biosens. Bioelectron.*, **150**, 111926.
16. Krause, S., Cerretani, C. and Vosch, T. (2019) Disentangling optically activated delayed fluorescence and upconversion fluorescence in DNA stabilized silver nanoclusters. *Chem. Sci.*, **10**, 5326–5331.
17. Du, X. and Jin, R. (2019) Atomically precise metal nanoclusters for catalysis. *ACS Nano*, **13**, 7383–7387.
18. Du, Y., Sheng, H., Astruc, D. and Zhu, M. (2020) Atomically precise noble metal nanoclusters as efficient catalysts: a bridge between structure and properties. *Chem. Rev.*, **120**, 526–622.
19. Liu, X., Wang, F., Aizen, R., Yehezkeili, O. and Willner, I. (2013) Graphene oxide/nucleic-acid-stabilized silver nanoclusters: functional hybrid materials for optical aptamer sensing and multiplexed analysis of pathogenic DNAs. *J. Am. Chem. Soc.*, **135**, 11832–11839.
20. Fang, B.Y., Li, C., An, J., Zhao, S.D., Zhuang, Z.Y., Zhao, Y.D. and Zhang, Y.X. (2018) HIV-related DNA detection through switching on hybridized quenched fluorescent DNA-Ag nanoclusters. *Nanoscale*, **10**, 5532–5538.
21. Feng, L., Liu, M., Liu, H., Fan, C., Cai, Y., Chen, L., Zhao, M., Chu, S. and Wang, H. (2018) High-throughput and sensitive fluorimetric strategy for microRNAs in blood using wettable microwells array and silver nanoclusters with red fluorescence enhanced by metal organic frameworks. *ACS Appl. Mater. Interfaces*, **10**, 23647–23656.
22. Xie, X.Y., Xiao, P., Cao, X., Fang, W.H., Cui, G. and Dolg, M. (2018) The origin of the photoluminescence enhancement of gold-doped silver nanoclusters: the importance of relativistic effects and heteronuclear gold-silver bonds. *Angew. Chem. Int. Ed. Engl.*, **57**, 9965–9969.
23. Zhang, J., Liu, Y., Zhi, X., Zhang, C., Liu, T.F. and Cui, D. (2018) DNA-templated silver nanoclusters locate microRNAs in the nuclei of gastric cancer cells. *Nanoscale*, **10**, 11079–11090.
24. Chen, Y., Phipps, M.L., Werner, J.H., Chakraborty, S. and Martinez, J.S. (2018) DNA templated metal nanoclusters: from emergent properties to unique applications. *Acc. Chem. Res.*, **51**, 2756–2763.
25. Tao, Y., Li, M., Ren, J. and Qu, X. (2015) Metal nanoclusters: novel probes for diagnostic and therapeutic applications. *Chem. Soc. Rev.*, **44**, 8636–8663.
26. Zheng, K., Setyawati, M.I., Lim, T.P., Leong, D.T. and Xie, J. (2016) Antimicrobial cluster bombs: silver nanoclusters packed with saptomycin. *ACS Nano*, **10**, 7934–7942.
27. Shi, C., Wang, J., Sushko, M.L., Qiu, W., Yan, X. and Liu, X.Y. (2019) Silk flexible electronics: from *Bombyx mori* silk Ag nanoclusters hybrid materials to mesoscopic memristors and synaptic emulators. *Adv. Funct. Mater.*, **29**, 1904777.
28. Lin, X., Liu, Y., Deng, J., Lyu, Y., Qian, P., Li, Y. and Wang, S. (2018) Multiple advanced logic gates made of DNA-Ag nanocluster and the application for intelligent detection of pathogenic bacterial genes. *Chem. Sci.*, **9**, 1774–1781.
29. Tao, Y., Li, M., Ren, J. and Qu, X. (2015) Metal nanoclusters: novel probes for diagnostic and therapeutic applications. *Chem. Soc. Rev.*, **44**, 8636–8663.
30. Shang, L., Dorlich, R.M., Trouillet, V., Bruns, M. and Nienhaus, G.U. (2012) Ultrasmall fluorescent silver nanoclusters: Protein adsorption and its effects on cellular responses. *Nano Res.*, **5**, 531–542.
31. Choi, S., Dickson, R.M. and Yu, J. (2012) Developing luminescent silver nanodots for biological applications. *Chem. Soc. Rev.*, **5**, 531–542.
32. Yu, J.H., Choi, S. and Dickson, R.M. (2009) Shuttle-based fluorogenic silver-cluster biolabels. *Angew. Chem. Int. Ed.*, **48**, 318–320.
33. Chatterjee, N., Eom, H.J. and Choi, J. (2014) Effects of silver nanoparticles on oxidative DNA damage-repair as a function of p38 MAPK status: a comparative approach using human Jurkat T cells and the nematode *Caenorhabditis elegans*. *Environ. Mol. Mutagen.*, **55**, 122–133.
34. AshaRani, P.V., Low Kah Mun, G., Hande, M.P. and Valiyaveetil, S. (2009) Cytotoxicity and genotoxicity of silver nanoparticles in human cells. *ACS Nano*, **3**, 279–290.
35. Kittler, S., Greulich, C., Diendorf, J., Köller, M. and Epple, M. (2010) Toxicity of silver nanoparticles increases during storage because of slow dissolution under release of silver ions. *Chem. Mater.*, **22**, 4548–4554.
36. Beer, C., Foldbjerg, R., Hayashi, Y., Sutherland, D.S. and Autrup, H. (2012) Toxicity of silver nanoparticles - nanoparticle or silver ion? *Toxicol. Lett.*, **208**, 286–292.
37. Parker, M.W., Botchan, M.R. and Berger, J.M. (2017) Mechanisms and regulation of DNA replication initiation in eukaryotes. *Crit. Rev. Biochem. Mol. Biol.*, **52**, 107–144.
38. Kelly, T. (2017) Historical perspective of eukaryotic DNA replication. *Adv. Exp. Med. Biol.*, **1042**, 1–41.
39. Macheret, M. and Halazonetis, T.D. (2015) DNA replication stress as a hallmark of cancer. *Annu Rev Pathol*, **10**, 425–448.
40. Fragkos, M., Ganier, O., Coulombe, P. and Mechali, M. (2015) DNA replication origin activation in space and time. *Nat. Rev. Mol. Cell Biol.*, **16**, 360–374.
41. Burgers, P.M.J. and Kunkel, T.A. (2017) Eukaryotic DNA replication fork. *Annu. Rev. Biochem.*, **86**, 417–438.
42. Deegan, T.D. and Diffley, J.F. (2016) MCM: one ring to rule them all. *Curr. Opin. Struct. Biol.*, **37**, 145–151.
43. Douglas, M.E., Ali, F.A., Costa, A. and Diffley, J.F.X. (2018) The mechanism of eukaryotic CMG helicase activation. *Nature*, **555**, 265–268.
44. Kurat, C.F., Yeeles, J.T.P., Patel, H., Early, A. and Diffley, J.F.X. (2017) Chromatin controls DNA replication origin selection, lagging-strand synthesis, and replication fork rates. *Mol. Cell*, **65**, 117–130.
45. Yeeles, J.T., Deegan, T.D., Janska, A., Early, A. and Diffley, J.F. (2015) Regulated eukaryotic DNA replication origin firing with purified proteins. *Nature*, **519**, 431–435.
46. Reuswig, K.U. and Pfander, B. (2019) Control of eukaryotic DNA replication initiation-mechanisms to ensure smooth transitions. *Genes (Basel)*, **10**, 99.
47. Sparks, J. and Walter, J.C. (2019) Extracts for analysis of DNA replication in a nucleus-free system. *Cold Spring Harb. Protoc.*, **2019**, doi:10.1101/pdb.prot097154.

48. Sannino, V., Pezzimenti, F., Bertora, S. and Costanzo, V. (2017) *Xenopus laevis* as model system to study DNA damage response and replication fork stability. *Methods Enzymol.*, **591**, 211–232.
49. Hoogenboom, W.S., Klein Douwel, D. and Knipscheer, P. (2017) *Xenopus* egg extract: a powerful tool to study genome maintenance mechanisms. *Dev. Biol.*, **428**, 300–309.
50. Blow, J.J. and Laskey, R.A. (2016) *Xenopus* cell-free extracts and their contribution to the study of DNA replication and other complex biological processes. *Int. J. Dev. Biol.*, **60**, 201–207.
51. Ying, C.Y. and Gautier, J. (2005) The ATPase activity of MCM2-7 is dispensable for pre-RC assembly but is required for DNA unwinding. *EMBO J.*, **24**, 4334–4344.
52. Dominguez-Sola, D., Ying, C.Y., Grandori, C., Ruggiero, L., Chen, B., Li, M., Galloway, D.A., Gu, W., Gautier, J. and Dalla-Favera, R. (2007) Non-transcriptional control of DNA replication by c-Myc. *Nature*, **448**, 445–451.
53. Aparicio, T., Baer, R., Gottesman, M. and Gautier, J. (2016) MRN, CtIP, and BRCA1 mediate repair of topoisomerase II-DNA adducts. *J. Cell Biol.*, **212**, 399–408.
54. Lebofsky, R., Takahashi, T. and Walter, J.C. (2009) DNA replication in nucleus-free *Xenopus* egg extracts. *Methods Mol. Biol.*, **521**, 229–252.
55. Yu, J., Choi, S. and Dickson, R.M. (2009) Shuttle-based fluorogenic silver-cluster biolabels. *Angew. Chem. Int. Ed. Engl.*, **48**, 318–320.
56. Shen, Z., Duan, H. and Frey, H. (2007) Water-soluble fluorescent Ag nanoclusters obtained from multiarm star poly(acrylic acid) as “molecular hydrogel” templates. *Adv. Mater.*, **19**, 349–352.
57. Tao, Y., Li, Z., Ju, E., Ren, J. and Qu, X. (2013) One-step DNA-programmed growth of CpG conjugated silver nanoclusters: a potential platform for simultaneous enhanced immune response and cell imaging. *Chem. Commun. (Camb.)*, **49**, 6918–6920.
58. Diez, I., Pusa, M., Kulmala, S., Jiang, H., Walther, A., Goldmann, A.S., Muller, A.H., Ikkala, O. and Ras, R.H. (2009) Color tunability and electrochemiluminescence of silver nanoclusters. *Angew. Chem. Int. Ed. Engl.*, **48**, 2122–2125.
59. Tao, Y., Ju, E., Ren, J. and Qu, X. (2015) Bifunctionalized mesoporous silica-supported gold nanoparticles: intrinsic oxidase and peroxidase catalytic activities for antibacterial applications. *Adv. Mater.*, **27**, 1097–1104.
60. Li, M., Tang, Z., Lv, S., Song, W., Hong, H., Jing, X., Zhang, Y. and Chen, X. (2014) Cisplatin crosslinked pH-sensitive nanoparticles for efficient delivery of doxorubicin. *Biomaterials*, **35**, 3851–3864.
61. Giordano-Coltart, J., Ying, C.Y., Gautier, J. and Hurwitz, J. (2005) Studies of the properties of human origin recognition complex and its Walker A motif mutants. *Proc. Natl. Acad. Sci. USA*, **102**, 69–74.
62. Shechter, D., Ying, C.Y. and Gautier, J. (2004) DNA unwinding is an Mcm complex-dependent and ATP hydrolysis-dependent process. *J. Biol. Chem.*, **279**, 45586–45593.
63. Srinivasan, S.V., Dominguez-Sola, D., Wang, L.C., Hyrien, O. and Gautier, J. (2013) Cdc45 is a critical effector of myc-dependent DNA replication stress. *Cell Rep.*, **3**, 1629–1639.
64. Smith, J., Mun Tho, L., Xu, N. and Gillespie, D.A. (2010) In: George, F.V.W. and George, K. (eds). *Advances in Cancer Research*. Academic Press, Vol. **108**, pp. 73–112.
65. Dai, Y. and Grant, S. (2010) New insights into checkpoint kinase 1 in the DNA damage response signaling network. *Clin. Cancer Res.*, **16**, 376–383.
66. Marheineke, K. and Hyrien, O. (2001) Aphidicolin triggers a block to replication origin firing in *Xenopus* egg extracts. *J. Biol. Chem.*, **276**, 17092–17100.
67. Gillespie, P.J., Gambus, A. and Blow, J.J. (2012) Preparation and use of *Xenopus* egg extracts to study DNA replication and chromatin associated proteins. *Methods*, **57**, 203–213.
68. Wang, W.L., Onikubo, T. and Shechter, D. (2019) Chromatin characterization in *Xenopus laevis* cell-free egg extracts and embryos. *Cold Spring Harb. Protoc.*, **2019**, doi:10.1101/pdb.prot099879.
69. Poirier, M.G. and Marko, J.F. (2003) In: *Current Topics in Developmental Biology*. Academic Press, Vol. **55**, pp. 75–141.
70. Hoogenboom, W.S., Klein Douwel, D. and Knipscheer, P. (2017) *Xenopus* egg extract: a powerful tool to study genome maintenance mechanisms. *Dev. Biol.*, **428**, 300–309.
71. Georgescu, R., Yuan, Z., Bai, L., de Luna Almeida Santos, R., Sun, J., Zhang, D., Yurieva, O., Li, H. and O'Donnell, M.E. (2017) Structure of eukaryotic CMG helicase at a replication fork and implications to replisome architecture and origin initiation. *Proc. Natl. Acad. Sci. U.S.A.*, **114**, E697–E706.
72. Bhat, K.P. and Cortez, D. (2018) RPA and RAD51: fork reversal, fork protection, and genome stability. *Nat. Struct. Mol. Biol.*, **25**, 446–453.
73. Li, N., Zhai, Y., Zhang, Y., Li, W., Yang, M., Lei, J., Tye, B.K. and Gao, N. (2015) Structure of the eukaryotic MCM complex at 3.8 Å. *Nature*, **524**, 186–191.
74. Bleichert, F., Botchan, M.R. and Berger, J.M. (2017) Mechanisms for initiating cellular DNA replication. *Science*, **355**, eaah6317.
75. Simon, N., Bochman, M.L., Seguin, S., Brodsky, J.L., Seibel, W.L. and Schwacha, A. (2013) Ciprofloxacin is an inhibitor of the Mcm2-7 replicative helicase. *Biosci. Rep.*, **33**, e00072.